

# From frustrated packing to tecton-driven porous molecular solids

C. A. Gunawardana,<sup>a</sup> A. S. Sinha,<sup>a</sup> E. W. Reinheimer<sup>b</sup> and C. B. Aakeröy<sup>\*a</sup>

<sup>a</sup> *Department of Chemistry, Kansas State University, Manhattan, Kansas 66506, United States.  
E-mail: aakeroy@ksu.edu*

<sup>b</sup> *Rigaku Americas Corporation, 9009 New Trails Drive, The Woodlands, Texas 77381, United States.*

## Supplementary Information

### CONTENTS

NMR spectra	2–12
IR spectra	12–17
MEP surfaces	18
Structures of precursors	18
Crystallographic data	19–22
References	22

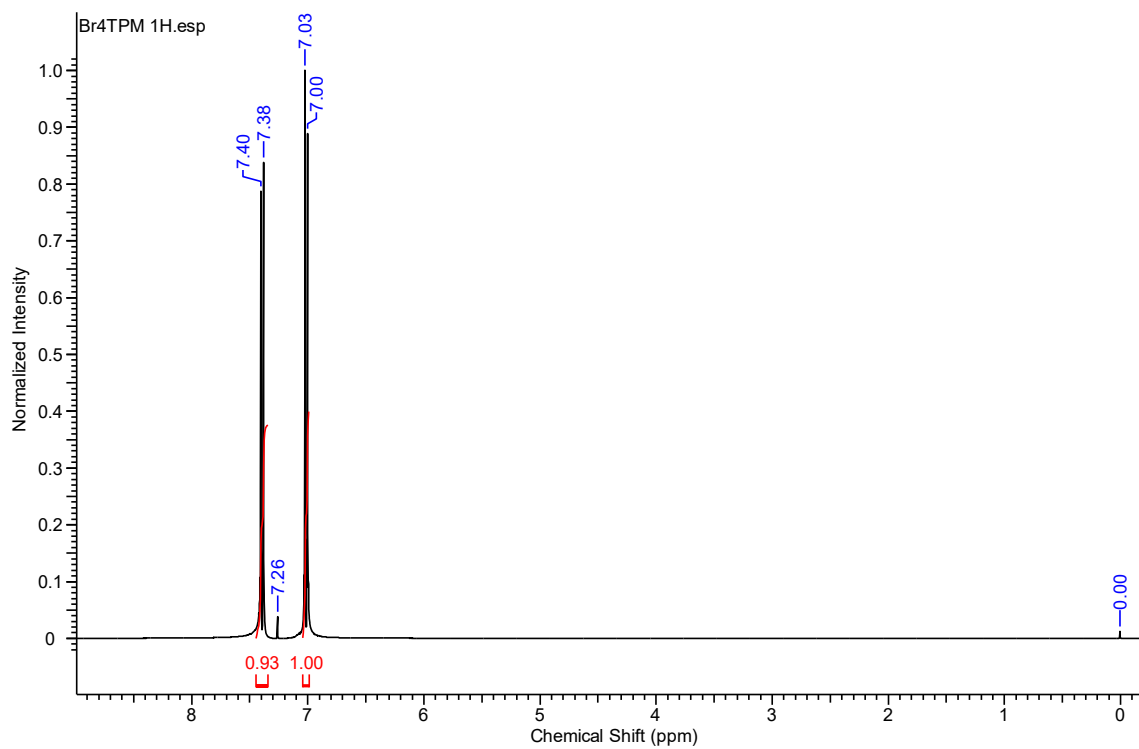


Figure S 1:  $^1\text{H}$ -NMR (400 MHz,  $\text{CDCl}_3$ ) spectrum of tetrakis(4-bromophenyl)methane ( $\text{Br}_4\text{TPM}$ ).

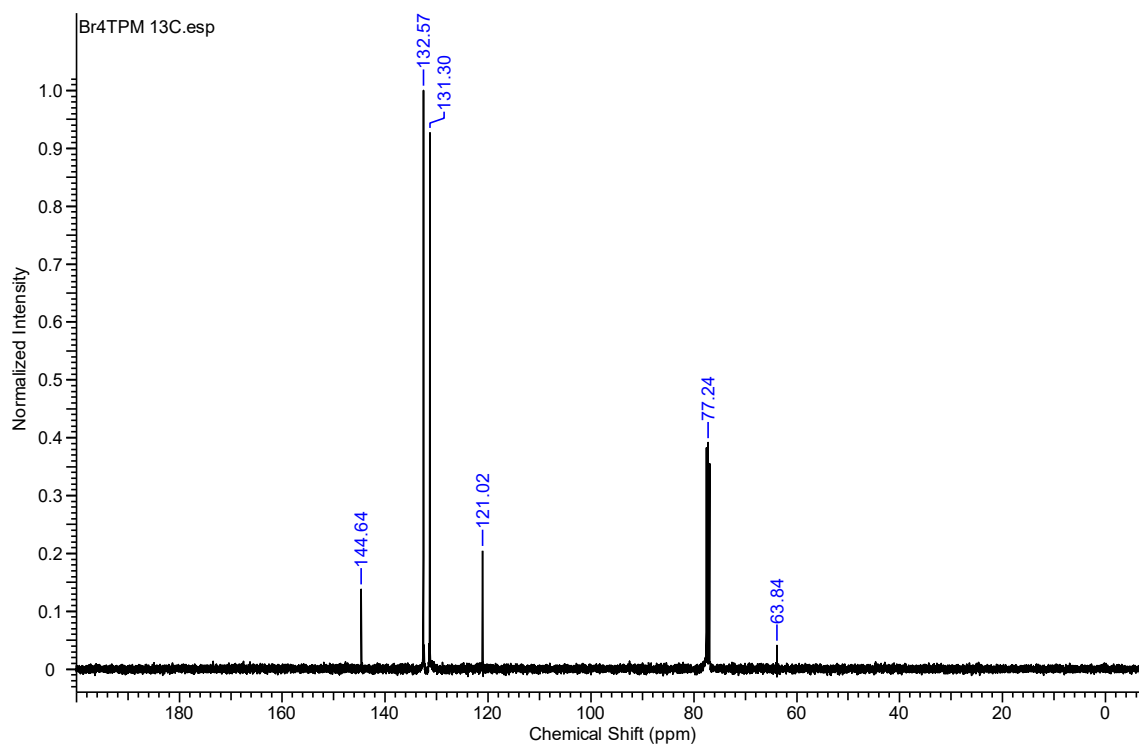


Figure S 2:  $^{13}\text{C}\{^1\text{H}\}$ -NMR (100 MHz,  $\text{CDCl}_3$ ) spectrum of tetrakis(4-bromophenyl)methane ( $\text{Br}_4\text{TPM}$ ).

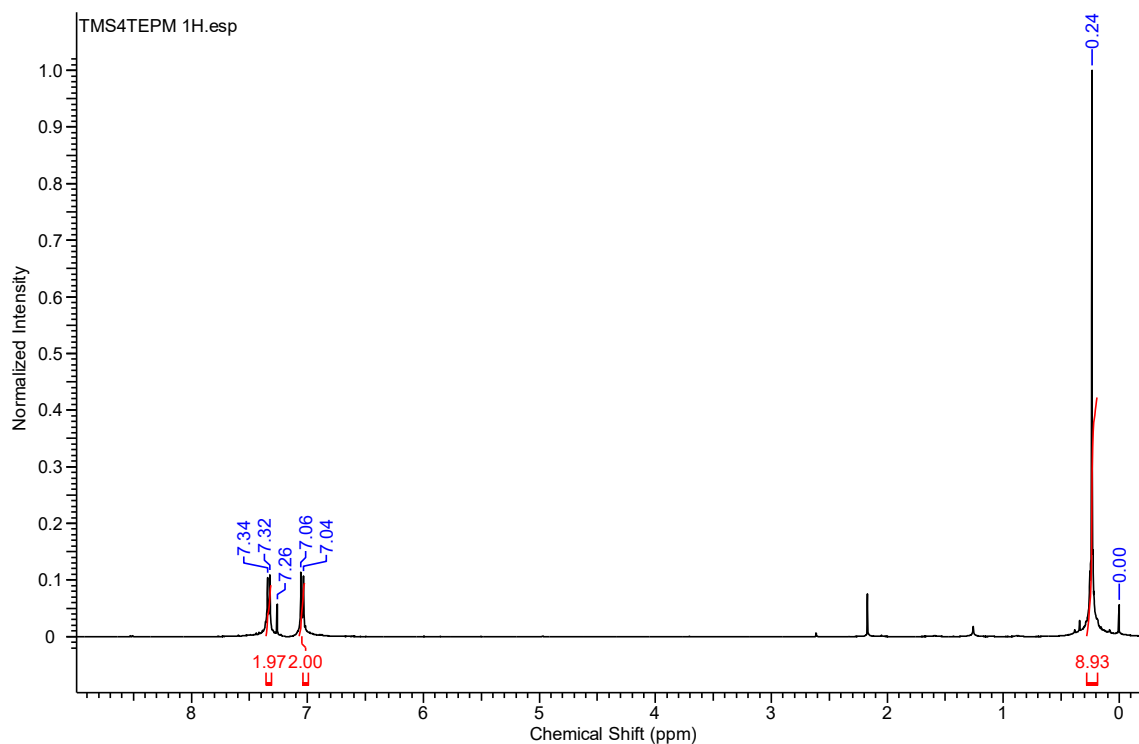


Figure 3: <sup>1</sup>H-NMR (400 MHz, CDCl<sub>3</sub>) spectrum of tetrakis(4-((trimethylsilyl)ethynyl)phenyl)methane (TMS<sub>4</sub>TEPM).

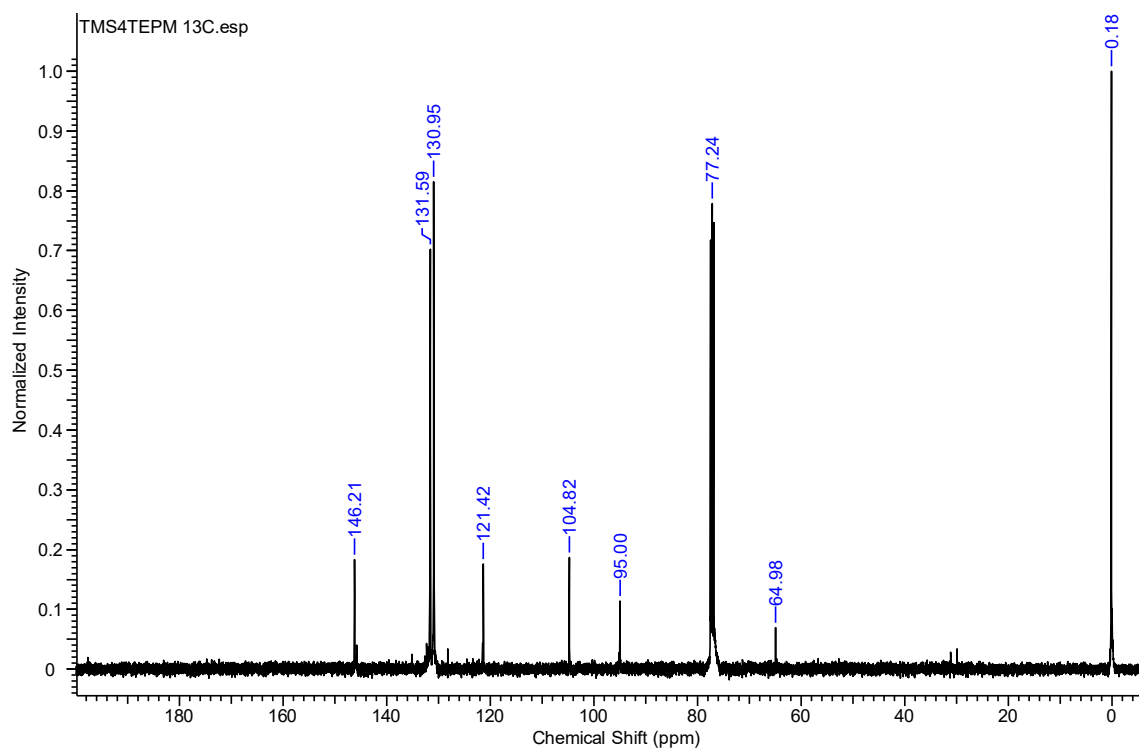


Figure 4: <sup>13</sup>C{<sup>1</sup>H}-NMR (100 MHz, CDCl<sub>3</sub>) spectrum of tetrakis(4-((trimethylsilyl)ethynyl)phenyl)methane (TMS<sub>4</sub>TEPM).

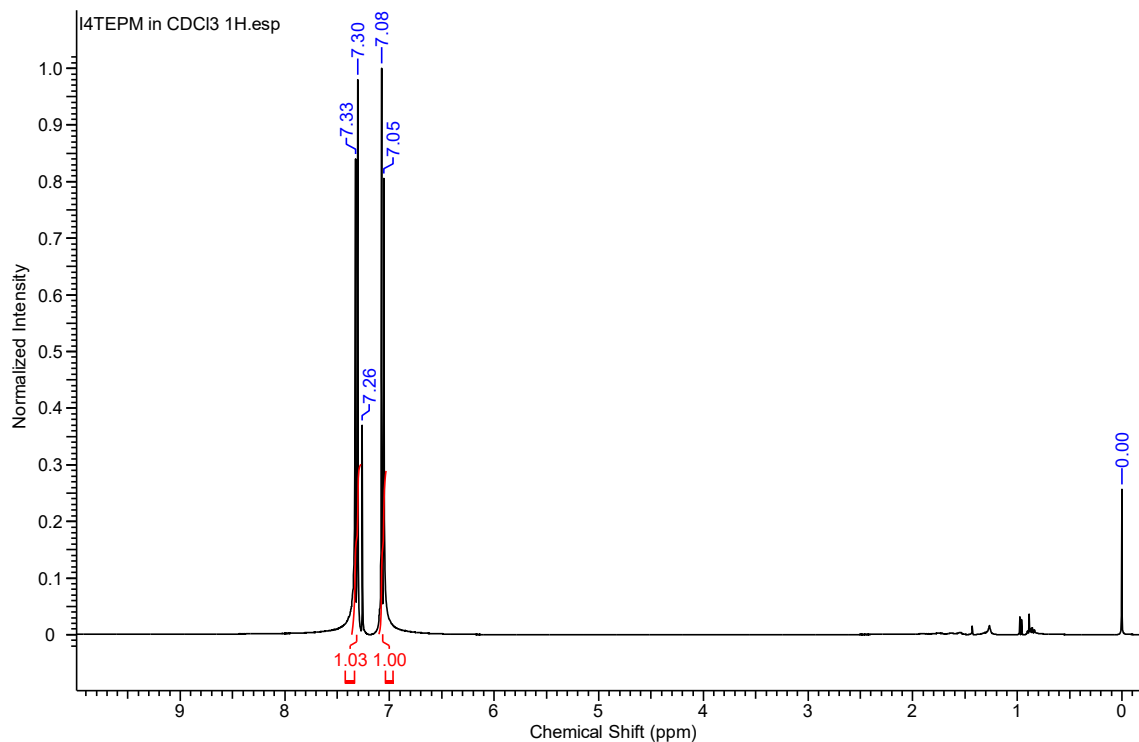


Figure S 5:  $^1\text{H-NMR}$  (400 MHz,  $\text{CDCl}_3$ ) spectrum of tetrakis(4-iodoethynyl)phenylmethane ( $\text{I}_4\text{TEPM}$ ).

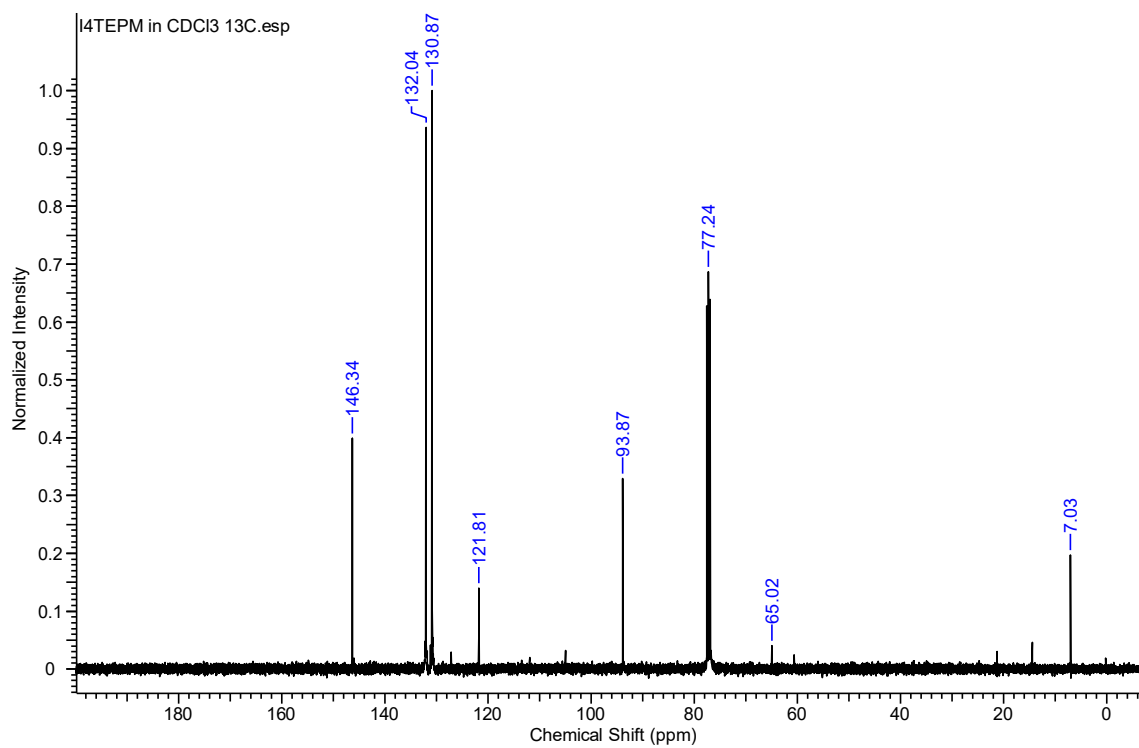
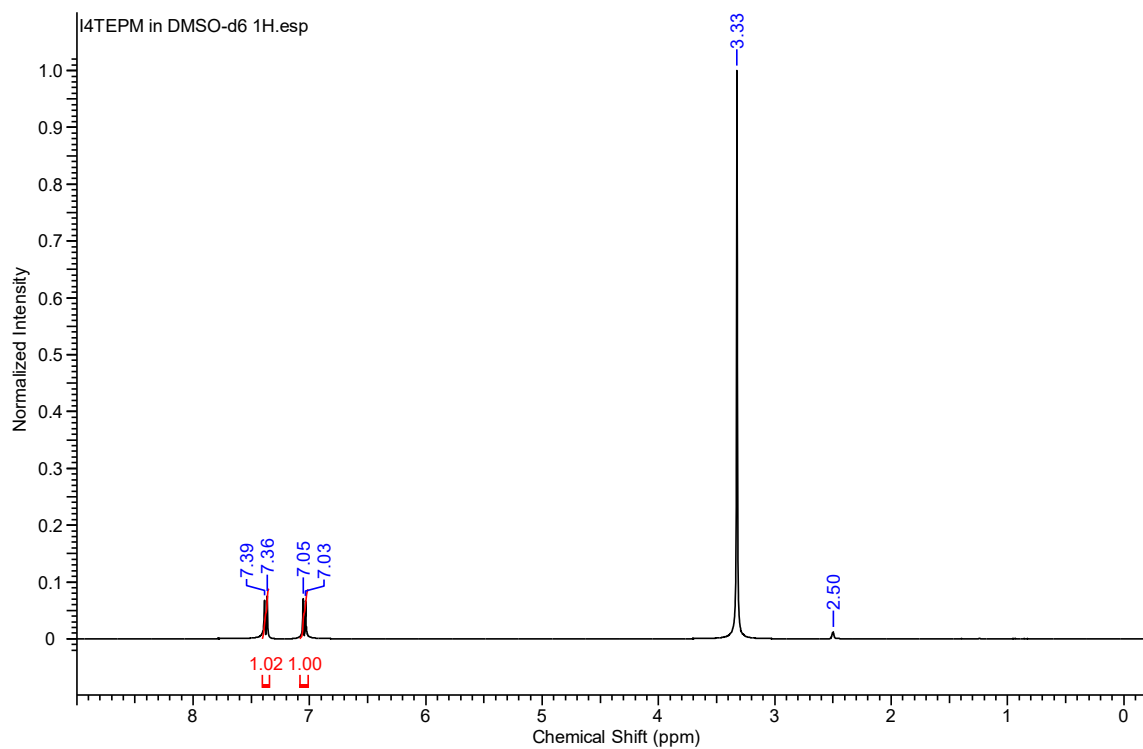
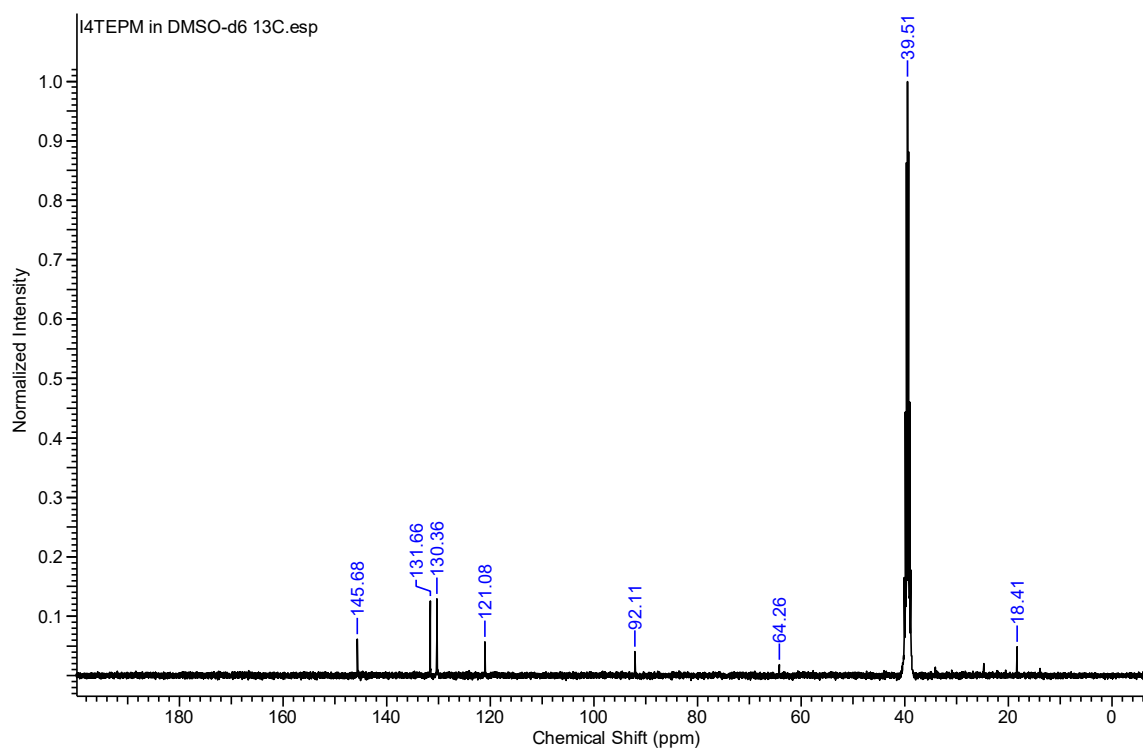


Figure S 6:  $^{13}\text{C}\{^1\text{H}\}$ -NMR (100 MHz,  $\text{CDCl}_3$ ) spectrum of tetrakis(4-iodoethynyl)phenylmethane ( $\text{I}_4\text{TEPM}$ ).



**Figure 7:**  $^1\text{H-NMR}$  (400 MHz,  $\text{DMSO-d}_6$ ) spectrum of tetrakis(4-(iodoethynyl)phenyl)methane ( $\text{I}_4\text{TEPM}$ ).



**Figure 8:**  $^{13}\text{C}\{^1\text{H}\}$ -NMR (100 MHz,  $\text{DMSO-d}_6$ ) spectrum of tetrakis(4-(iodoethynyl)phenyl)methane ( $\text{I}_4\text{TEPM}$ ).

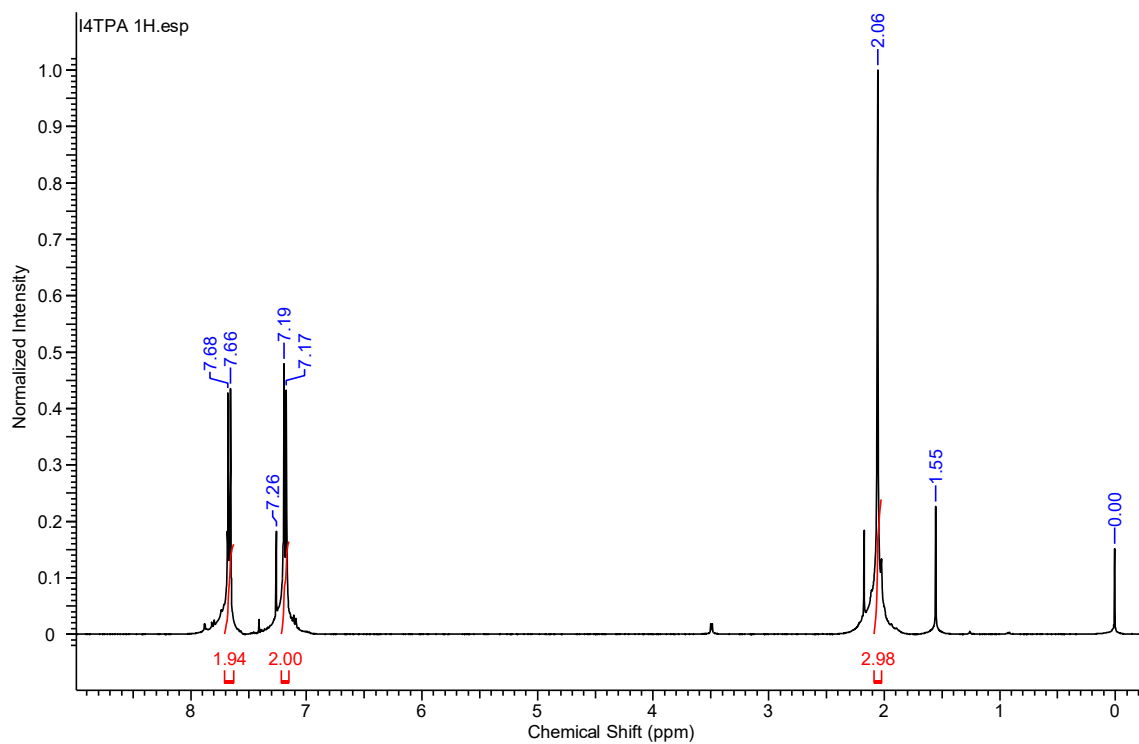


Figure 9:  $^1\text{H-NMR}$  (400 MHz,  $\text{CDCl}_3$ ) spectrum of 1,3,5,7-tetrakis(4-iodophenyl)adamantane ( $I_4\text{TPA}$ ).

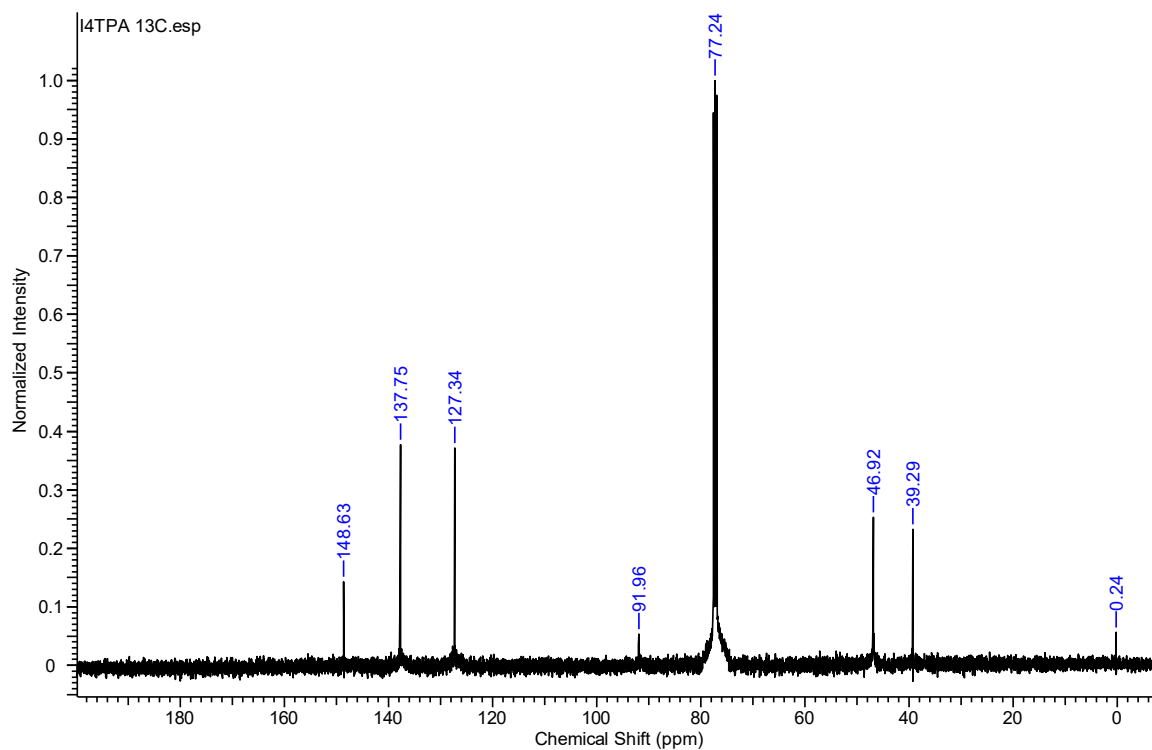


Figure 10:  $^{13}\text{C}\{^1\text{H}\}$ -NMR (100 MHz,  $\text{CDCl}_3$ ) spectrum of 1,3,5,7-tetrakis(4-iodophenyl)adamantane ( $I_4\text{TPA}$ ).

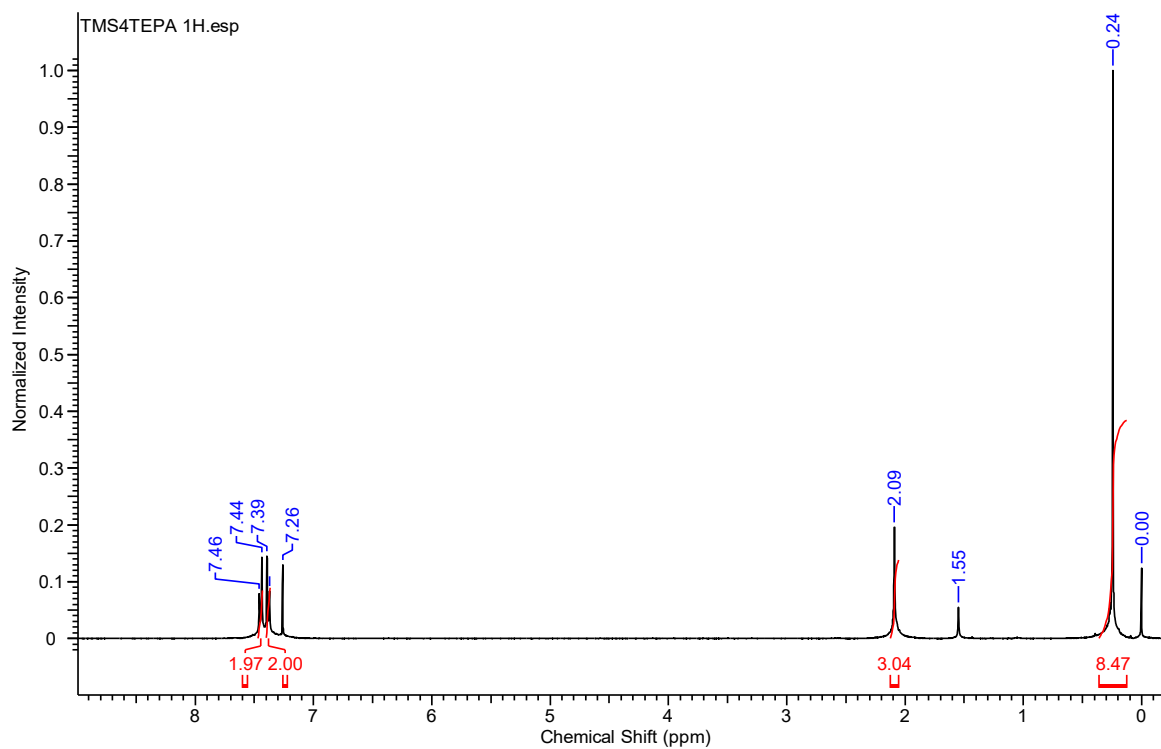


Figure S 11:  $^1\text{H-NMR}$  (400 MHz,  $\text{CDCl}_3$ ) spectrum of 1,3,5,7-tetrakis(4-((trimethylsilyl)ethynyl)phenyl)adamantane ( $\text{TMS}_4\text{TEPA}$ ).

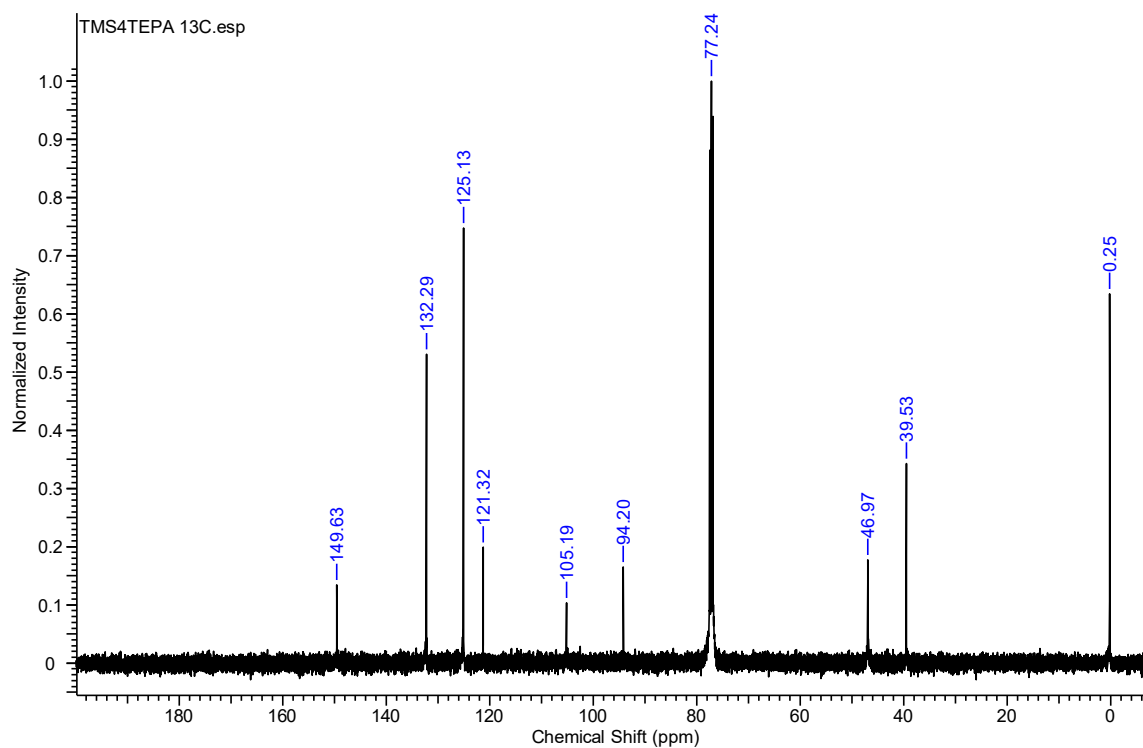


Figure S 12:  $^{13}\text{C}\{^1\text{H}\}$ -NMR (100 MHz,  $\text{CDCl}_3$ ) spectrum of 1,3,5,7-tetrakis(4-((trimethylsilyl)ethynyl)phenyl)adamantane ( $\text{TMS}_4\text{TEPA}$ ).

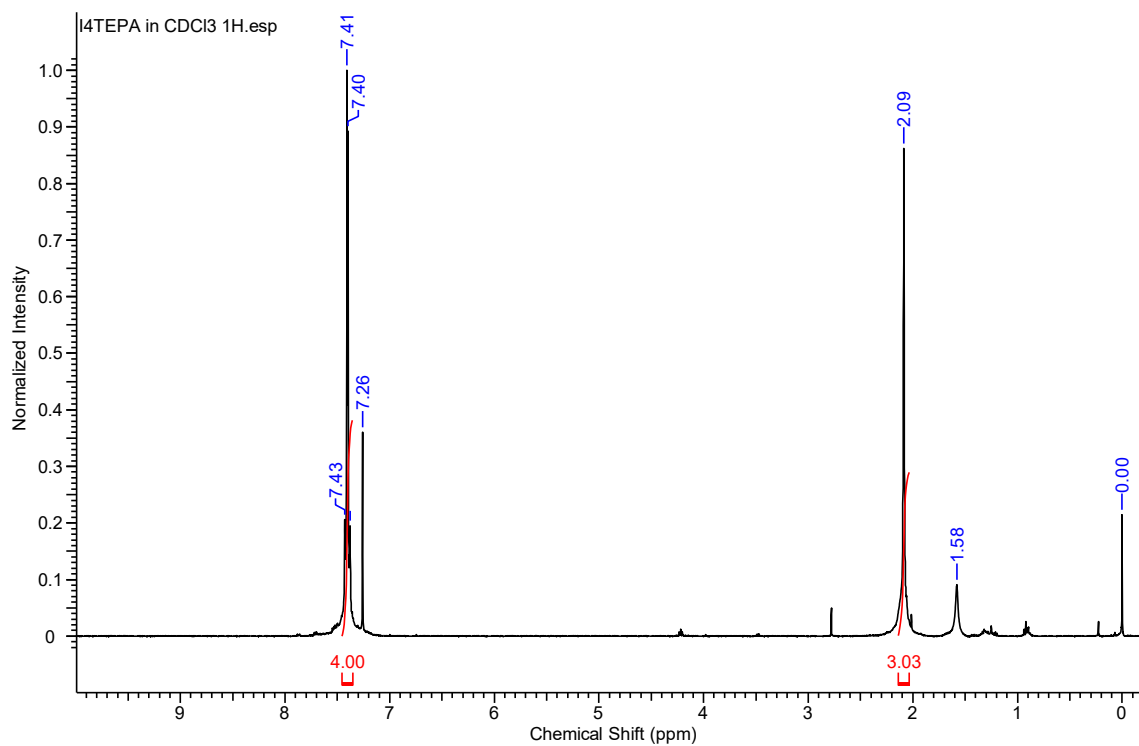


Figure S 13:  $^1\text{H-NMR}$  (400 MHz,  $\text{CDCl}_3$ ) spectrum of 1,3,5,7-tetrakis(4-(iodoethynyl)phenyl)adamantane ( $\text{I}_4\text{TEPA}$ ).

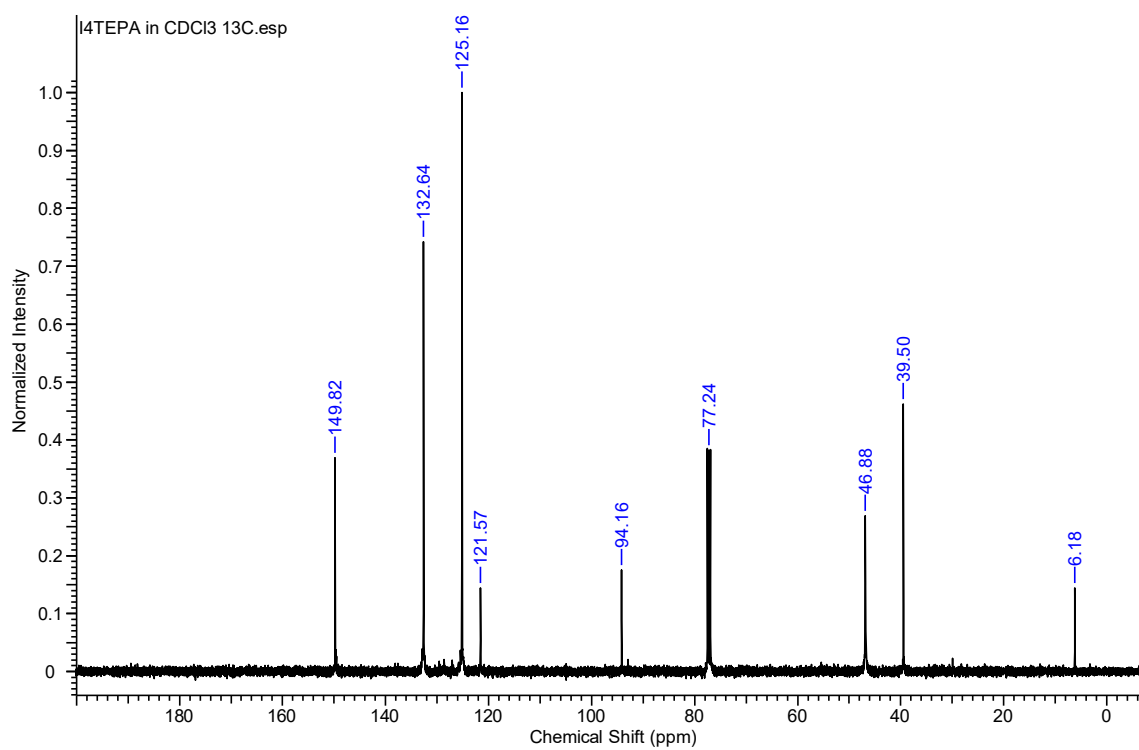


Figure S 14:  $^{13}\text{C}\{^1\text{H}\}$ -NMR (100 MHz,  $\text{CDCl}_3$ ) spectrum of 1,3,5,7-tetrakis(4-(iodoethynyl)phenyl)adamantane ( $\text{I}_4\text{TEPA}$ ).

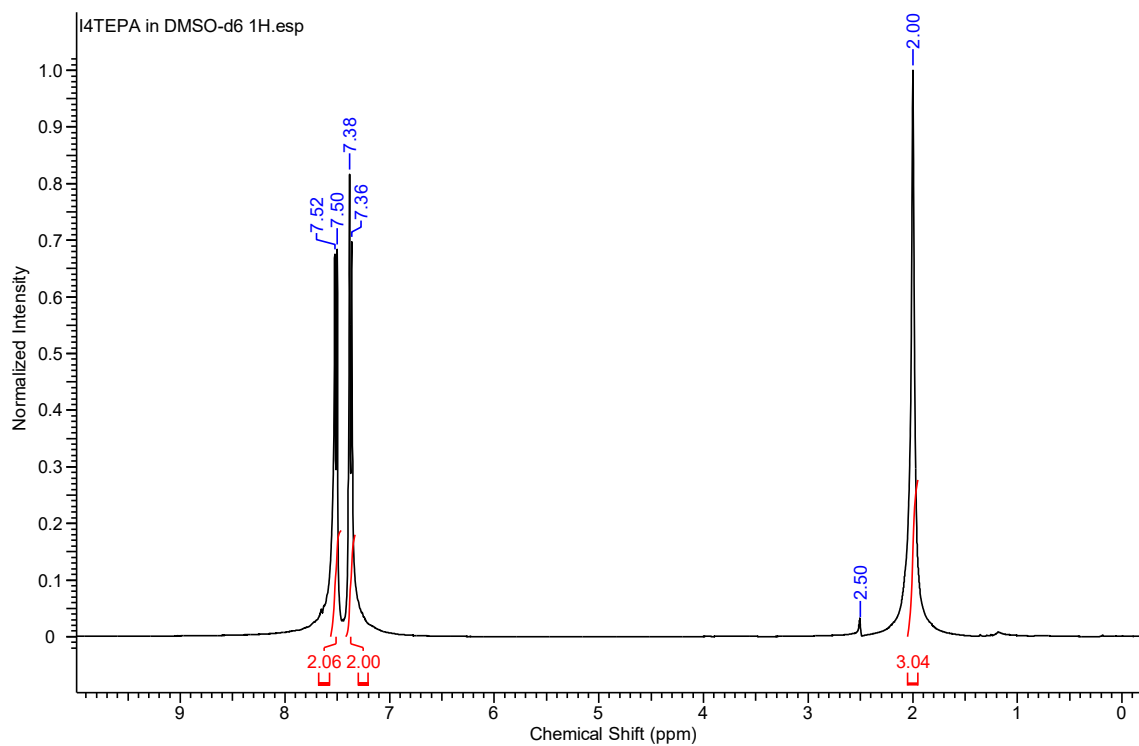


Figure S 15:  $^1\text{H-NMR}$  (400 MHz,  $\text{DMSO-d}_6$ ) spectrum of 1,3,5,7-tetrakis(4-(iodoethynyl)phenyl)adamantane ( $\text{I}_4\text{TEPA}$ ).

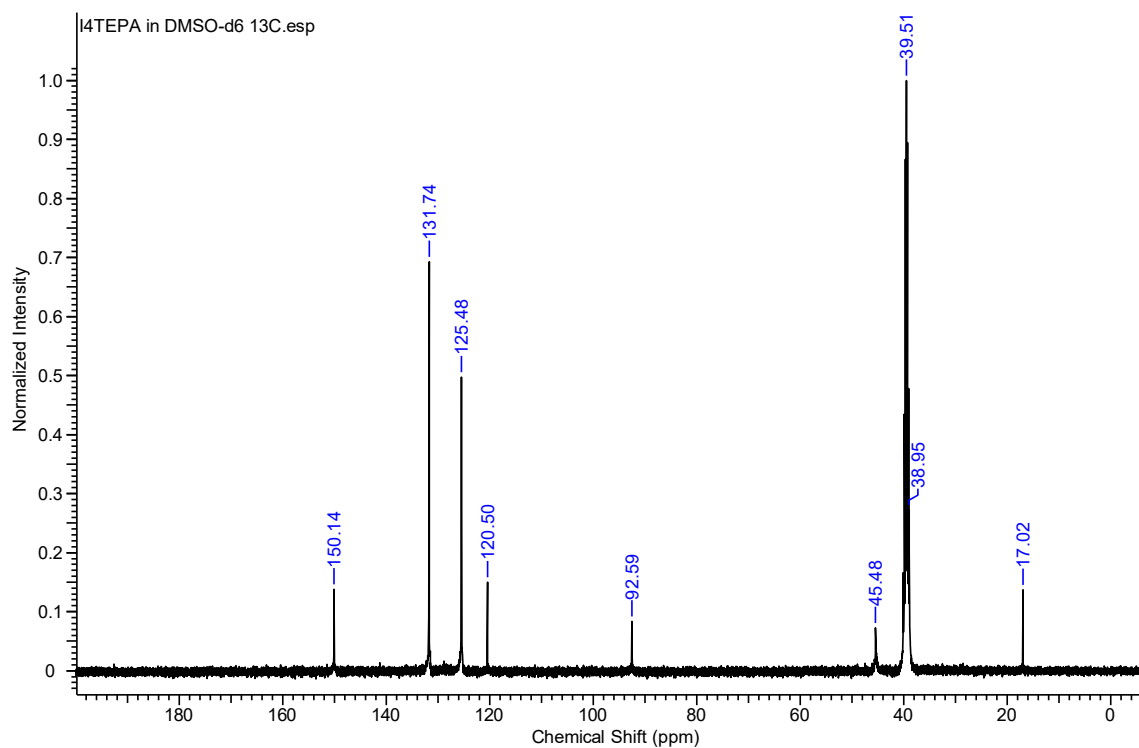


Figure S 16:  $^{13}\text{C}\{^1\text{H}\}$ -NMR (100 MHz,  $\text{DMSO-d}_6$ ) spectrum of 1,3,5,7-tetrakis(4-(iodoethynyl)phenyl)adamantane ( $\text{I}_4\text{TEPA}$ ).

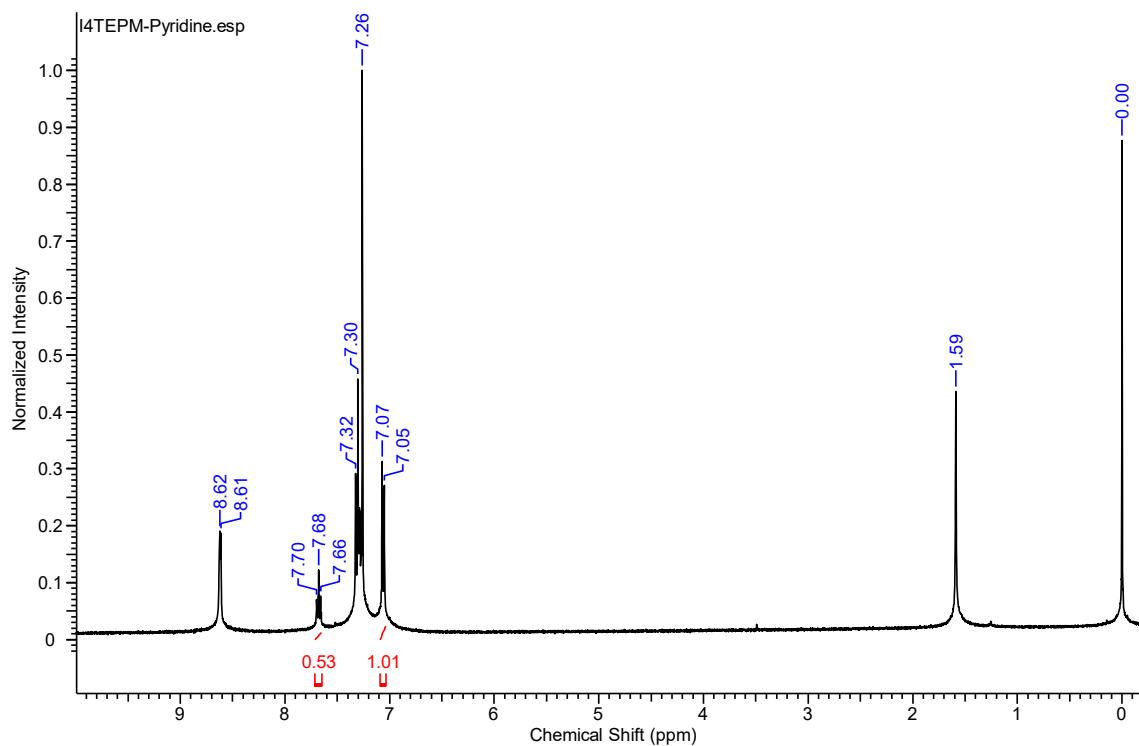


Figure S 17:  $^1\text{H-NMR}$  (400 MHz,  $\text{CDCl}_3$ ) spectrum of  $\text{I}_4\text{TEPM}\cdot 4\text{pyridine}$  crystals.

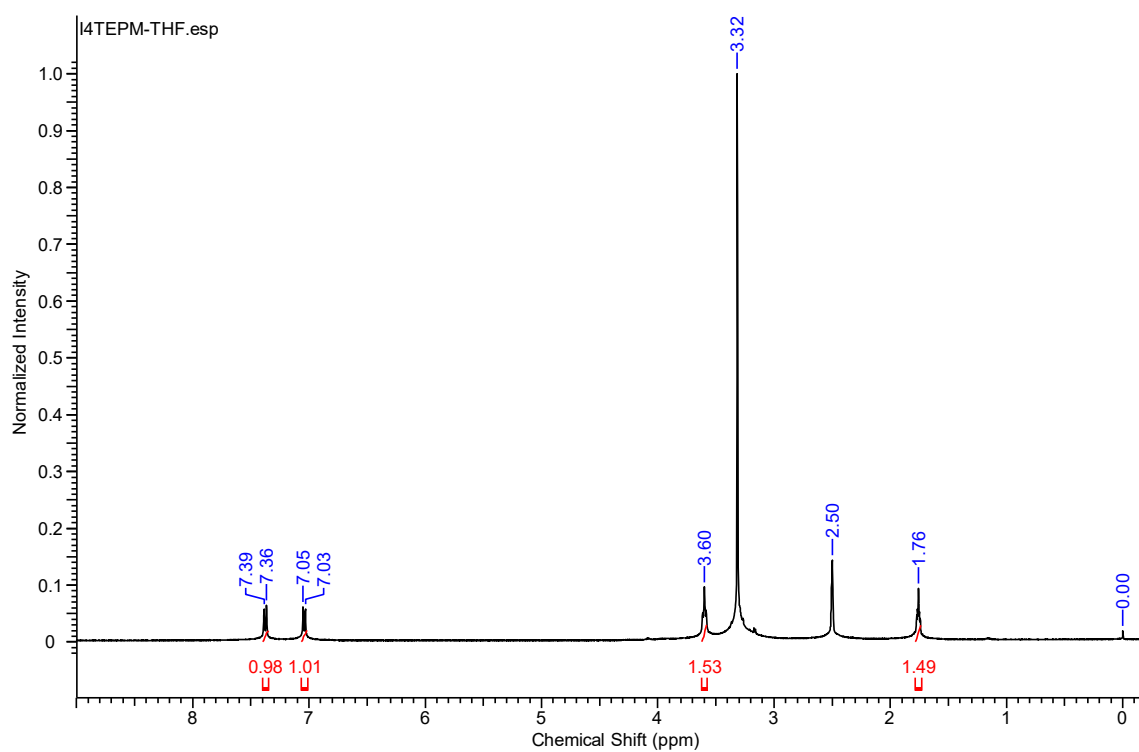


Figure S 18:  $^1\text{H-NMR}$  (400 MHz,  $\text{DMSO-d}_6$ ) spectrum of  $\text{I}_4\text{TEPM}\cdot 2\text{THF}$  crystals.

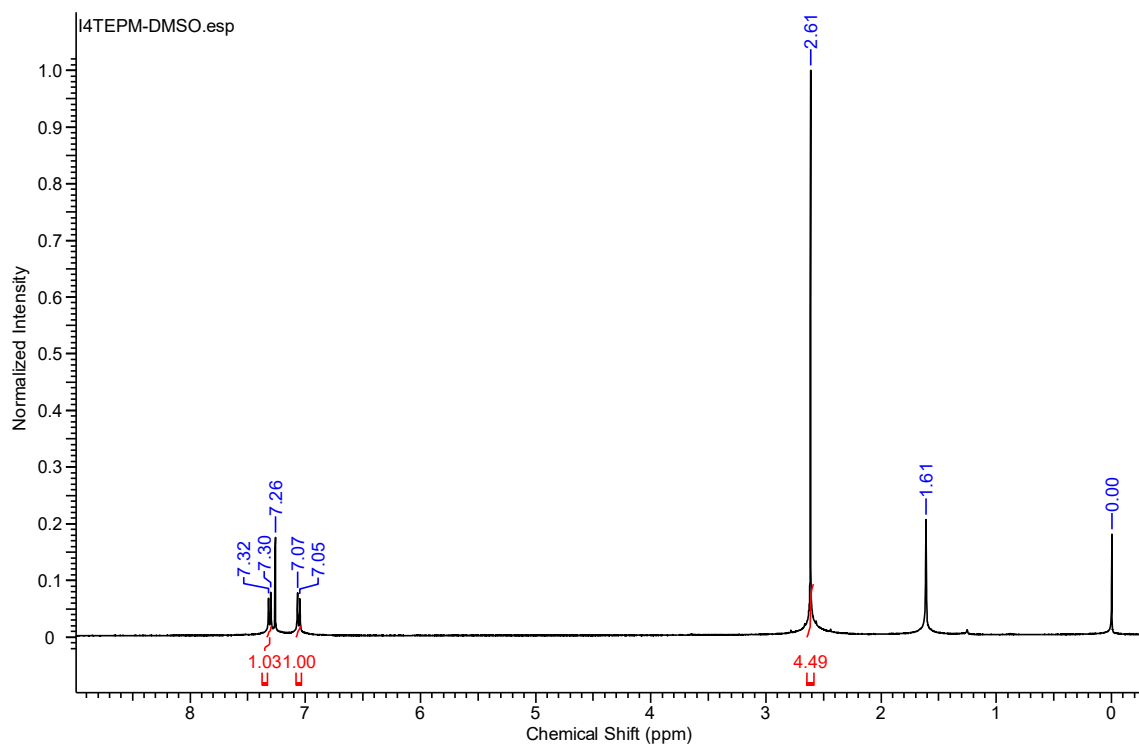


Figure S 19:  $^1\text{H-NMR}$  (400 MHz,  $\text{CDCl}_3$ ) spectrum of  $\text{I}_4\text{TEPM}\cdot 2\text{DMSO}$  crystals.

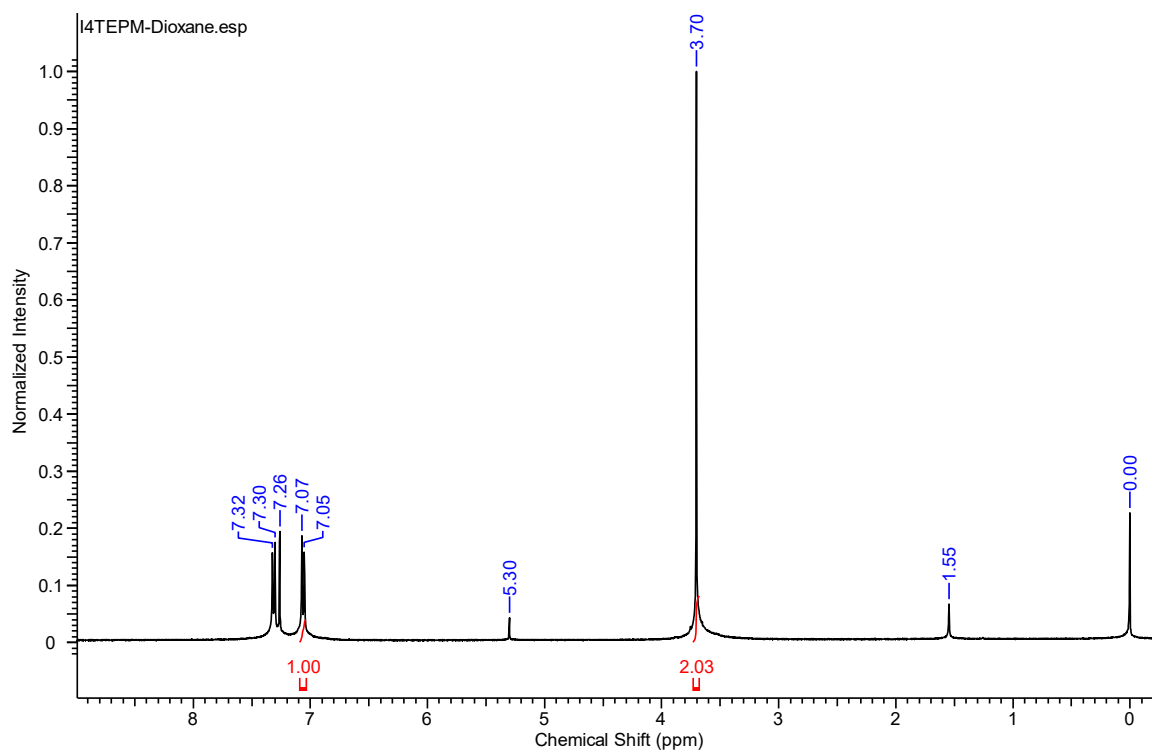


Figure S 20:  $^1\text{H-NMR}$  (400 MHz,  $\text{CDCl}_3$ ) spectrum of  $\text{I}_4\text{TEPM}\cdot 2\text{dioxane}$  crystals.

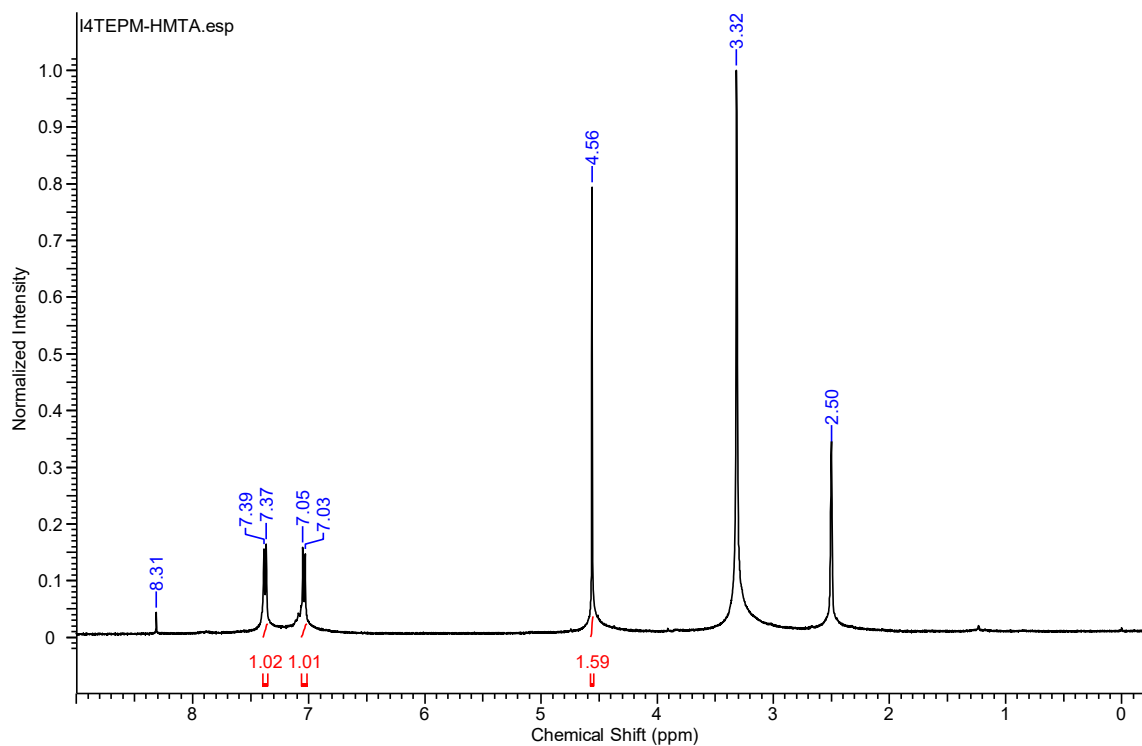


Figure S 21:  $^1\text{H-NMR}$  (400 MHz,  $\text{DMSO-d}_6$ ) spectrum of  $\text{I}_4\text{TEPM-HMTA}$  microcrystals.

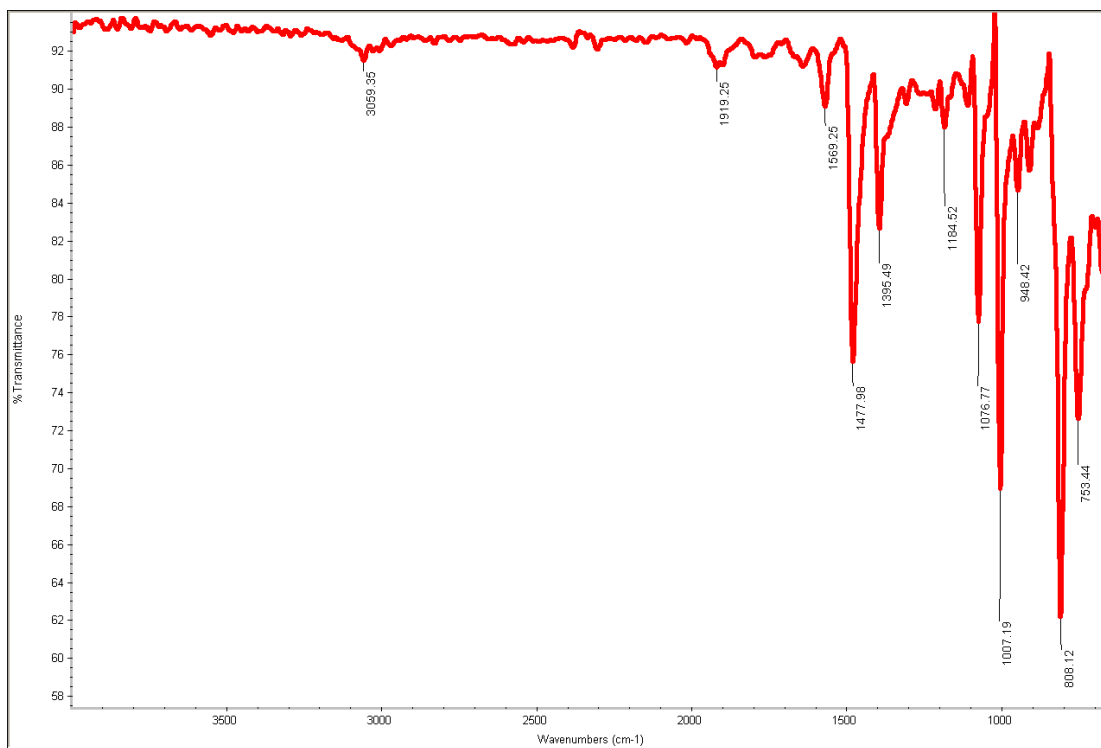


Figure S 22: ATR-FTIR spectrum of tetrakis(4-bromophenyl)methane ( $\text{Br}_4\text{TPM}$ ).

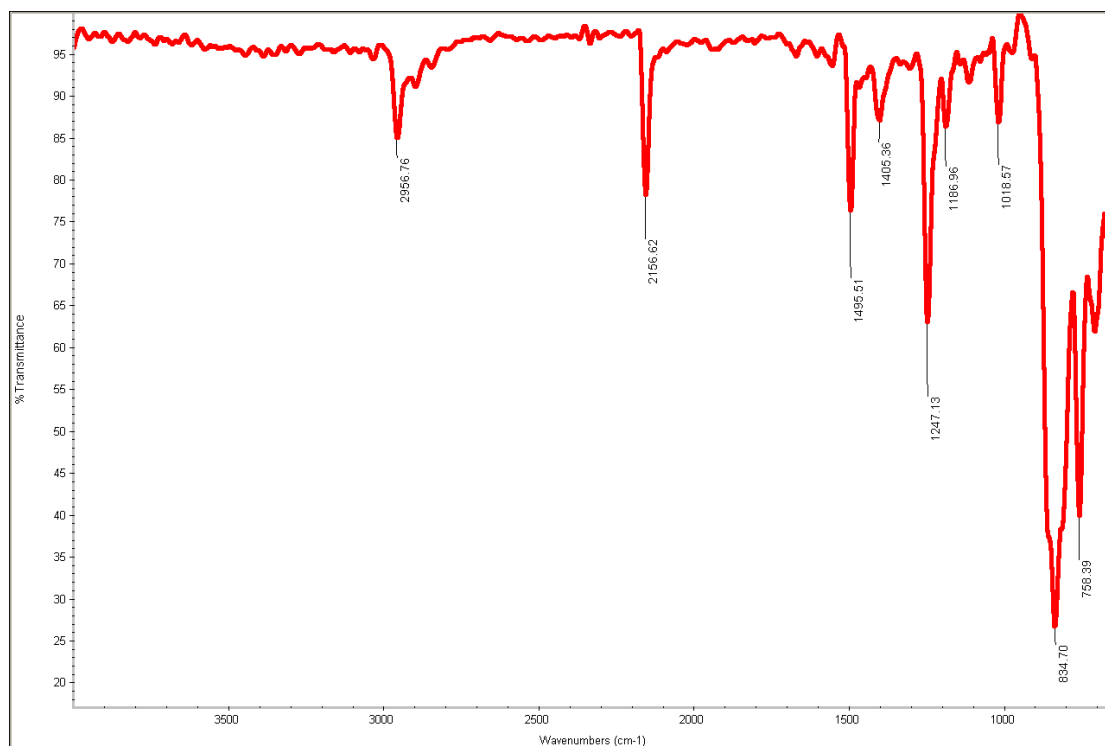


Figure S 23: ATR-FTIR spectrum of tetrakis(4-((trimethylsilyl)ethynyl)phenyl)methane ( $TMS_4TEPM$ ).

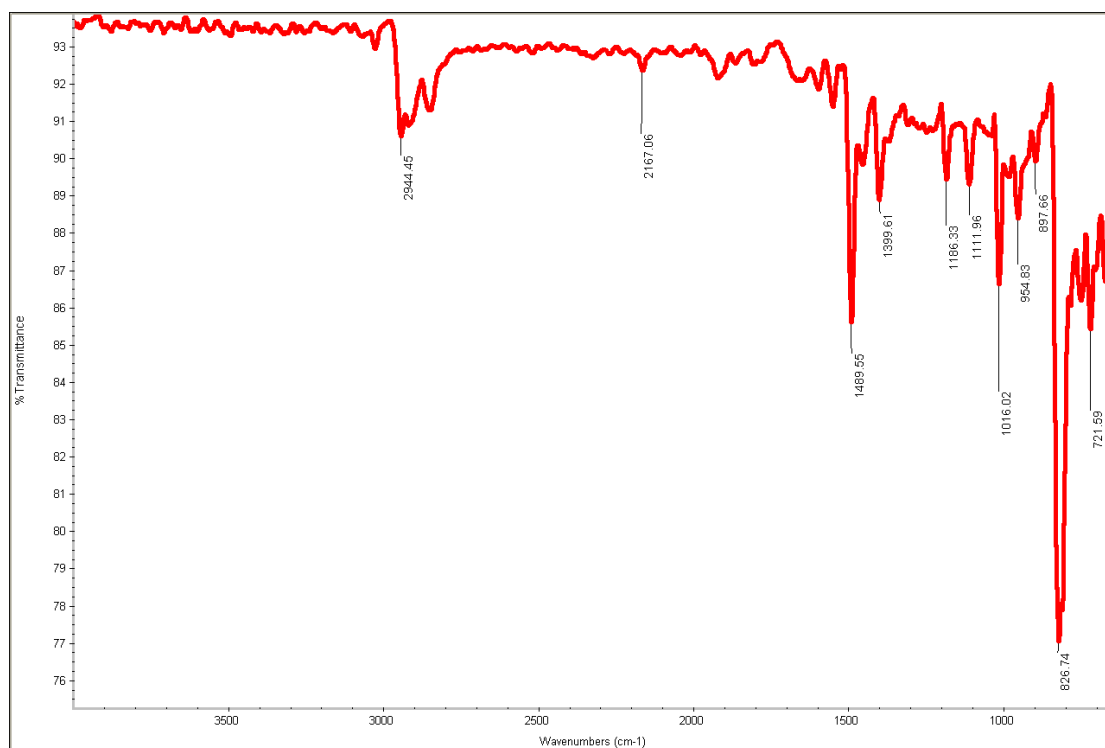


Figure S 24: ATR-FTIR spectrum of tetrakis(4-(iodoethynyl)phenyl)methane ( $I_4TEPM$ ).

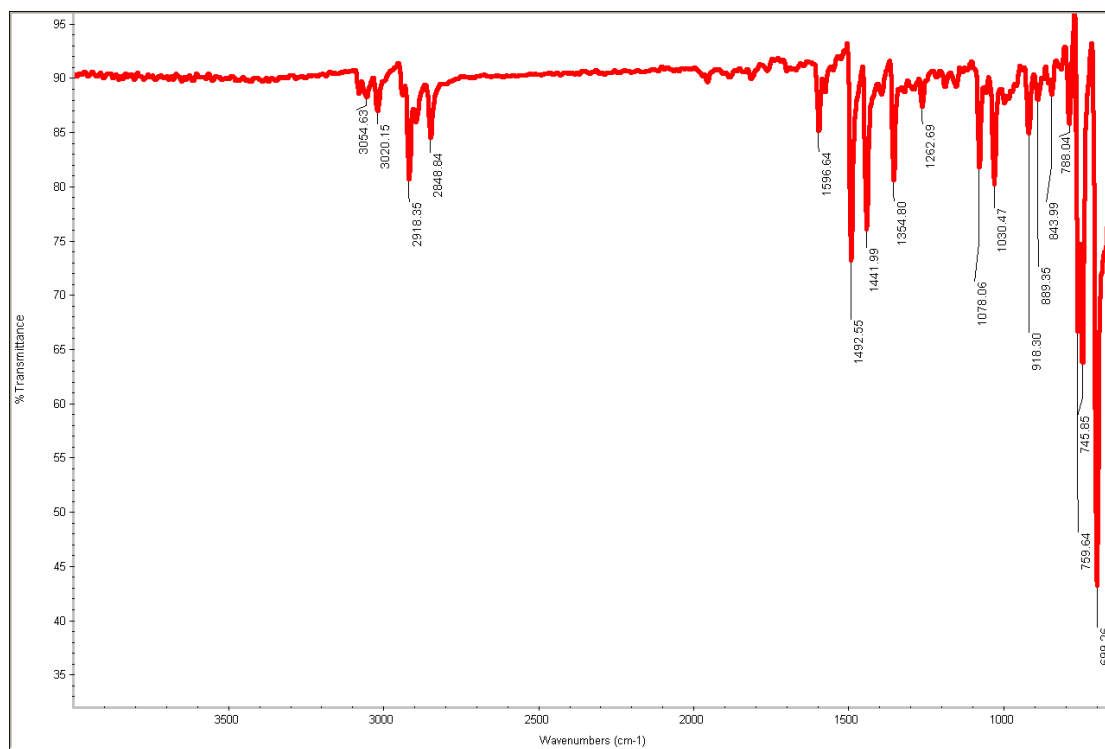


Figure S 25: ATR-FTIR spectrum of 1,3,5,7-tetraphenyladamantane (TPA).

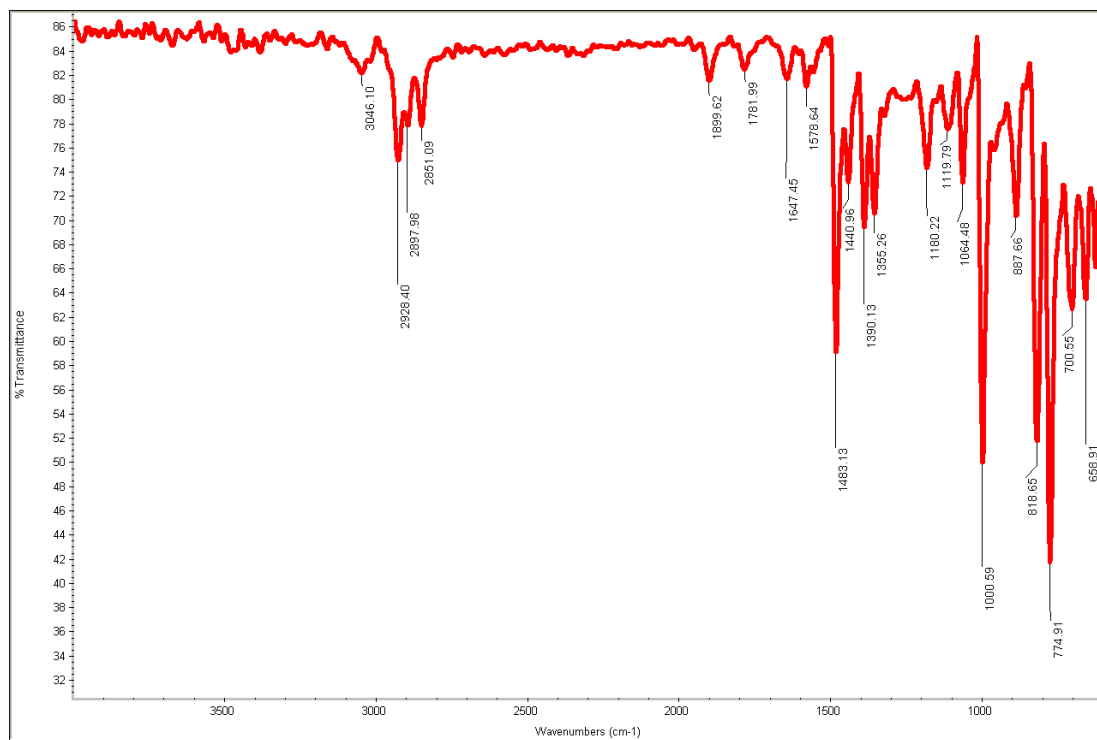


Figure S 26: ATR-FTIR spectrum of 1,3,5,7-tetrakis(4-iodophenyl)adamantane (I<sub>4</sub>TPA).

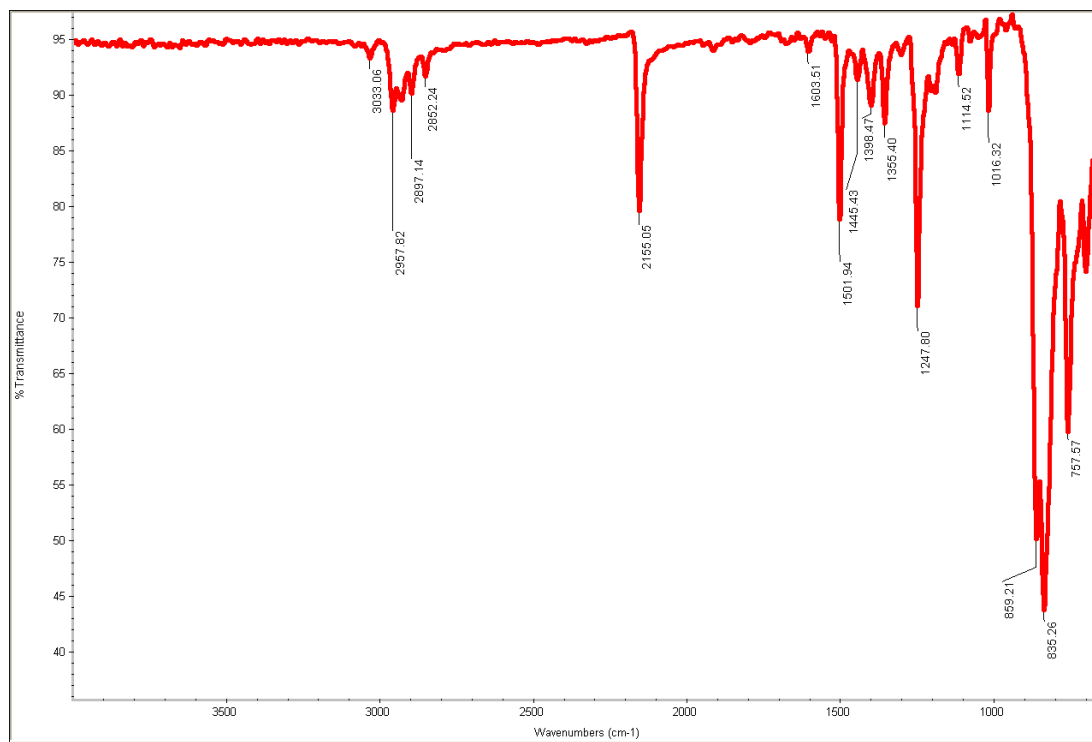


Figure S 27: ATR-FTIR spectrum of 1,3,5,7-tetrakis(4-((trimethylsilyl)ethynyl)phenyl)adamantane ( $TMS_4TEPA$ ).

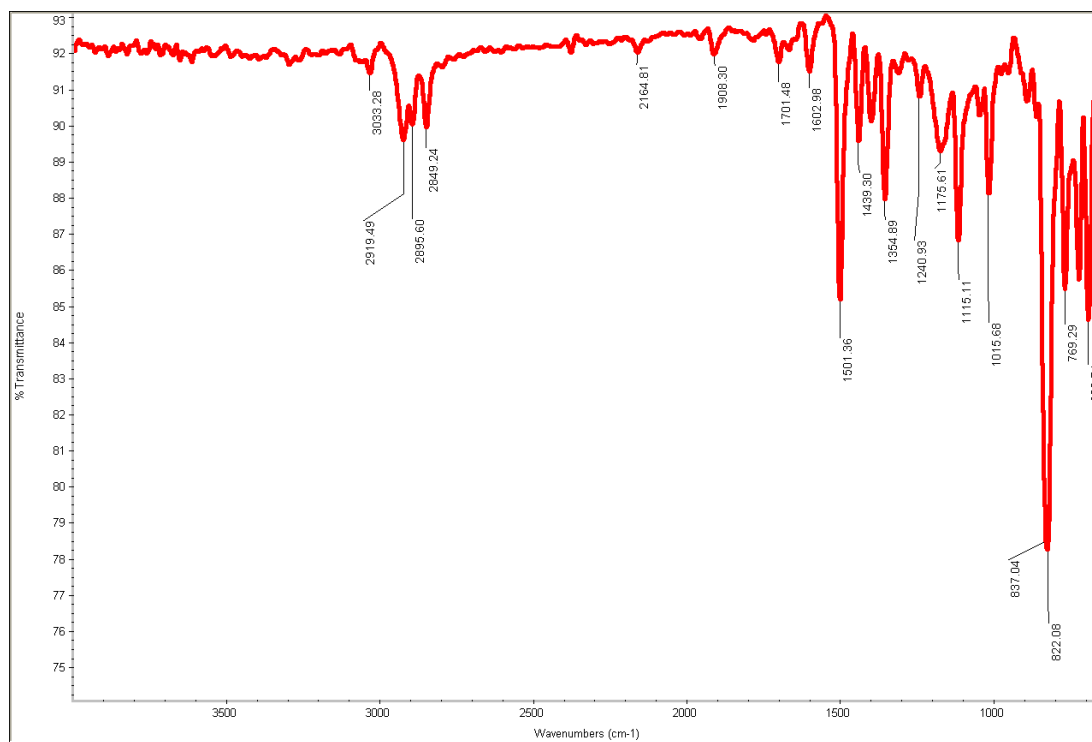


Figure S 28: ATR-FTIR spectrum of 1,3,5,7-tetrakis(4-(iodoethyl)phenyl)adamantane ( $I_4TEPA$ ).

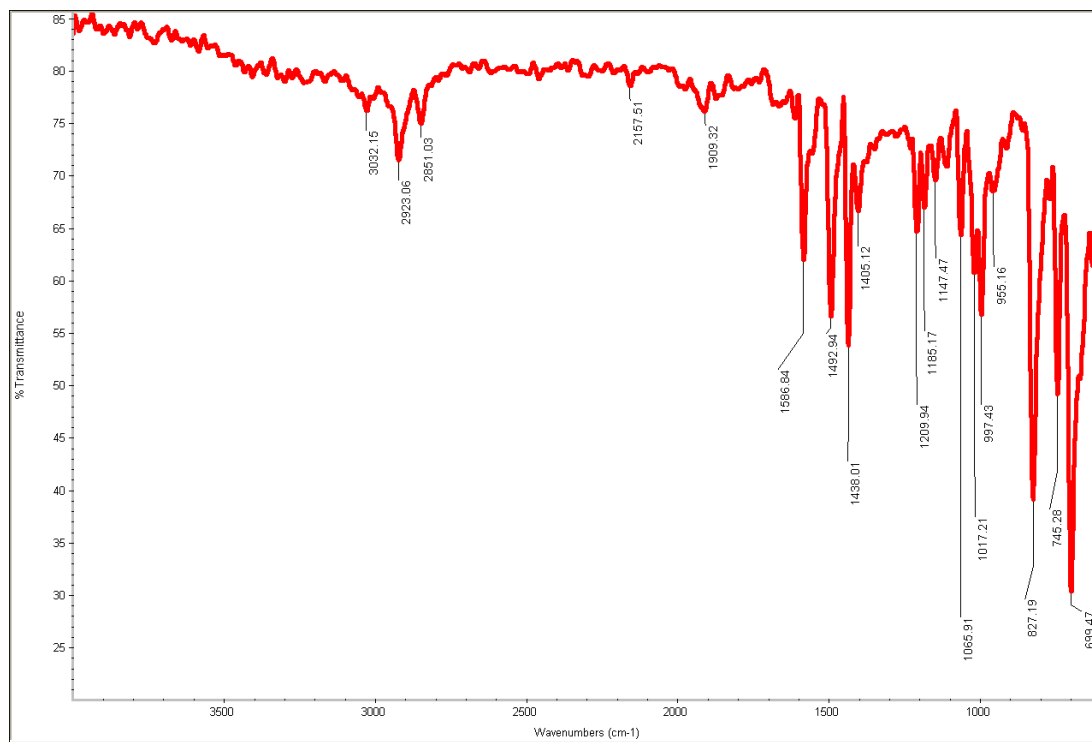


Figure S 29: ATR-FTIR spectrum of  $I_4TEPM \cdot 4pyridine$  crystals.

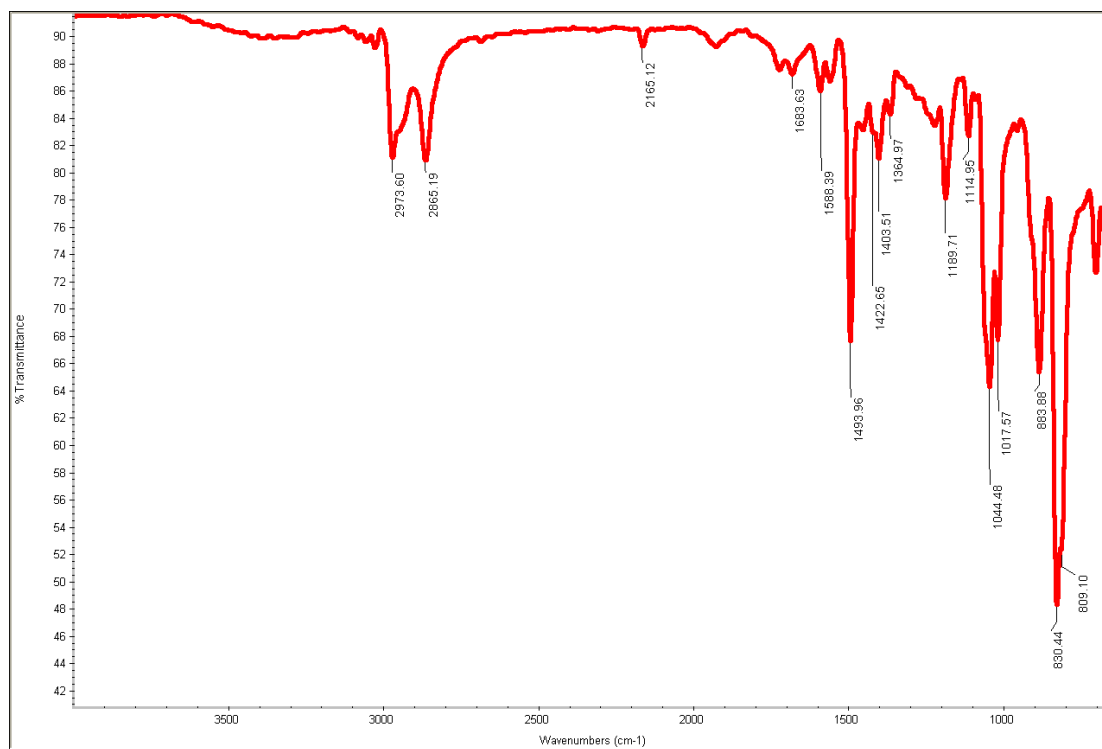


Figure S 30: ATR-FTIR spectrum of  $I_4TEPM \cdot 2THF$  crystals.

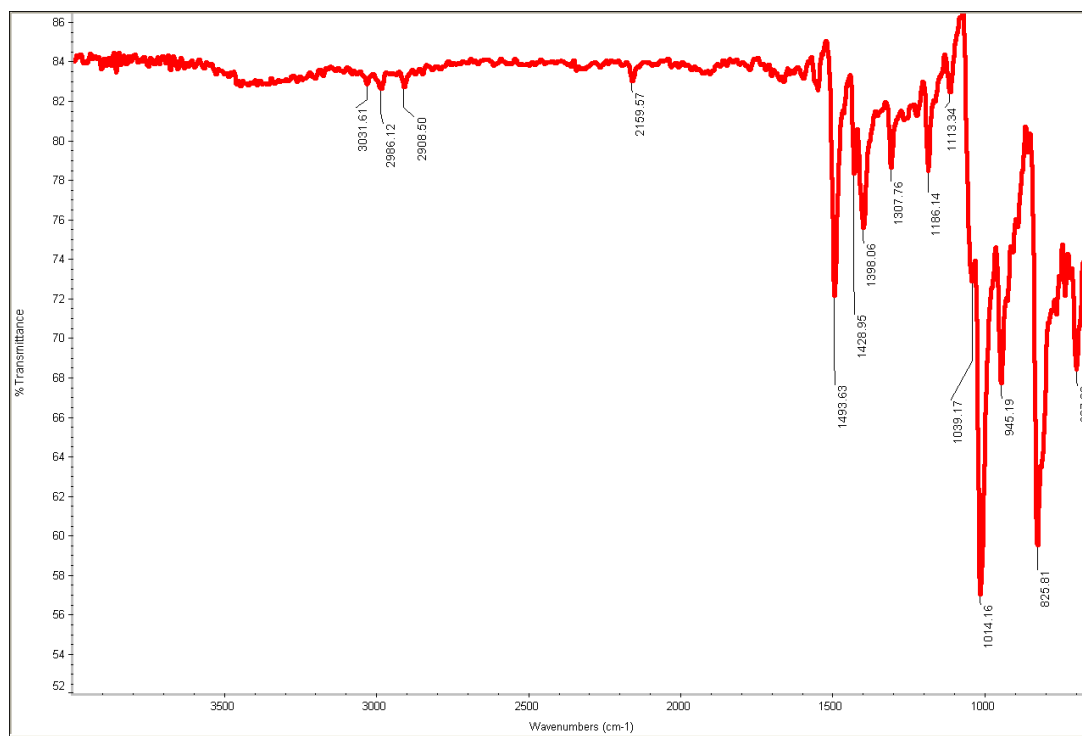


Figure S 31: ATR-FTIR spectrum of  $I_4TEPM \cdot 2DMSO$  crystals.

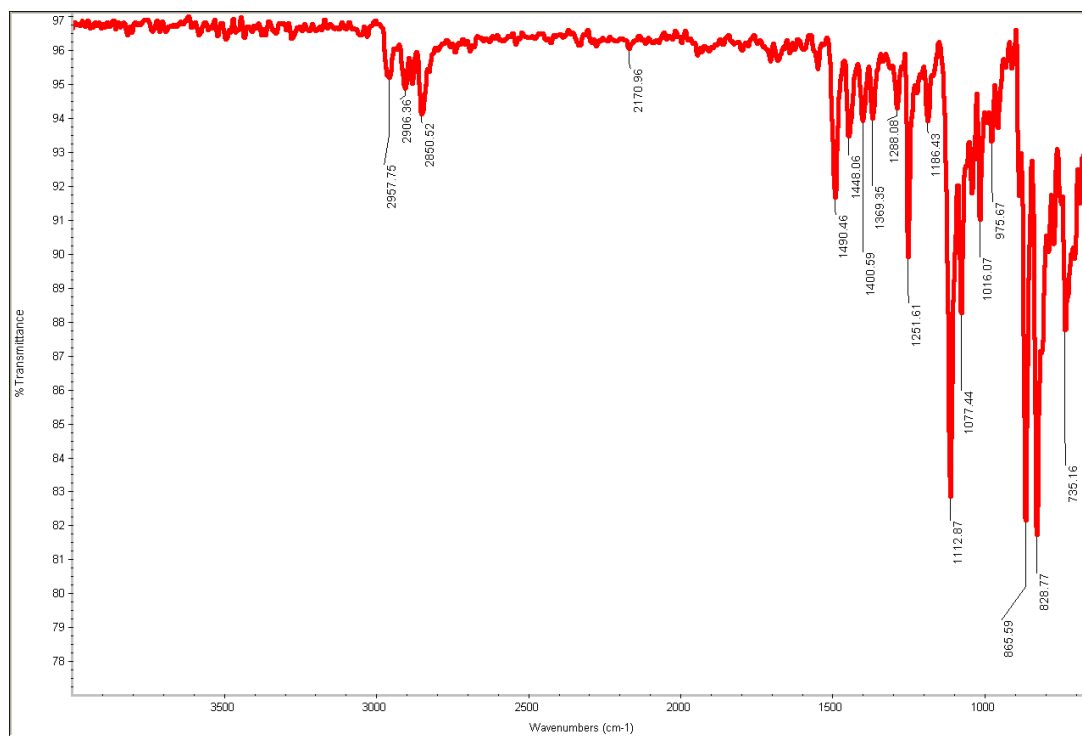
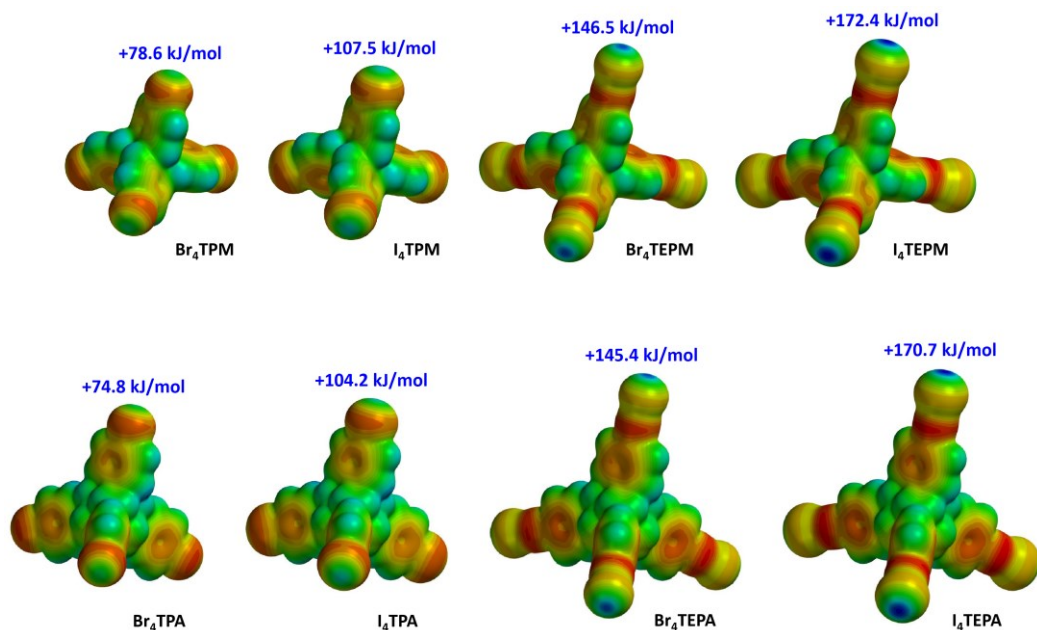


Figure S 32: ATR-FTIR spectrum of  $I_4TEPM \cdot 2dioxane$  crystals.

## Electrostatic potential calculations

In order to calculate the molecular electrostatic potentials (MEPs) of tetra-halogenated TPM and TPA species, first, their geometries were optimized using Spartan '14 software. Geometry optimizations of TPM derivatives were carried out at hybrid functional B3LYP/6-311+G\*\* level of theory. For TPA derivatives, B3LYP/6-311++G\*\* level was used. The visualization of MEPs was subsequently attained through mapping its values onto 0.002 au isosurface, determined with a positive point charge in the vacuum as a probe. The numbers, now termed surface potentials, indicate the Coulombic interaction energies (expressed in kJ/mol) between the probe and this isodensity surface at different points.



**Figure S 33:** MEP surfaces of tetra-halogenated TPM and TPA species with their  $\sigma$ -hole potentials. All plots have been set to the same color scale for visual comparison. Range: from  $-80$  kJ/mol (red) to  $+175$  kJ/mol (blue).

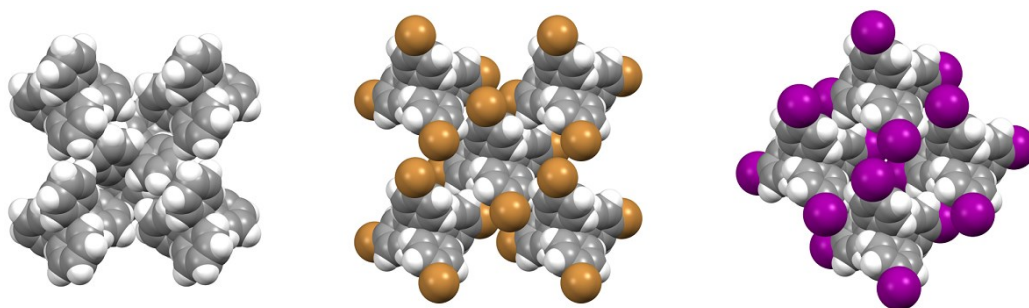


**Figure S 34:** Densely-packed structures of (from left) TPM, Br<sub>4</sub>TPM and I<sub>4</sub>TPM.

## Single-crystal X-ray diffraction

Datasets were collected on a Bruker Kappa APEX II system using MoK $\alpha$  radiation (**I4TEPM.THF**; **I4TEPM.DMSO**), or on a Bruker MicroStar Rotating Anode system using CuK $\alpha$  radiation (**I4TEPM**). Data were collected using APEX2 software.<sup>1</sup> Initial cell constants were found by small widely separated “matrix” runs. Data collection strategies were determined using COSMO.<sup>2</sup> Scan speed and scan widths were chosen based on scattering power and peak rocking curves. Datasets were collected at 23°C (**I4TEPM**), and at -143°C (**I4TEPM.THF**; **I4TEPM.DMSO**) using an Oxford Cryostream low-temperature device.

For the above datasets, the unit cell constants and orientation matrix were improved by least-squares refinement of reflections thresholded from the entire dataset. Integration was performed with SAINT,<sup>3</sup> using this improved unit cell as a starting point. Precise unit cell constants were calculated in SAINT from the final merged dataset. Lorentz and polarization corrections were applied. Multi-scan absorption corrections were performed with SADABS.<sup>4</sup>

For the above datasets, data were reduced with ShelXTL.<sup>5</sup> The structures were solved in all cases by intrinsic phasing methods without incident. Also, the structures were solved and finalized using OLEX2 1.2 suite of program.<sup>6,7</sup> Except as noted, hydrogen atoms were located in idealized positions and were treated with a riding model. All non-hydrogen atoms were assigned anisotropic thermal parameters. Refinements continued to convergence, using the recommended weighting schemes.

Disordered solvent molecules were present in structures **I4TEPM**, **I4TEPM.THF**, and **I4TEPM.DMSO**. It was difficult to determine the identity of these solvent molecules. Consequently, the automatic “solvent masking procedure” present in OLEX2 1.2 was used to mask the solvent molecules present in these structures.<sup>6,7</sup> According to the applied solvent mask, the void in the structure **I4TEPM** was 1000.4 Å<sup>3</sup>, and the void consisted of a total of 43.2 electrons. Based on the electron count present in the void, it is hypothesized that there are possibly four water molecules present in the crystal lattice. The void in **I4TEPM.THF** is 677.6 Å<sup>3</sup>, and it consists of a total of 205.6 electrons. Based on the electron count present in the void, it is hypothesized that there are possibly five tetrahydrofuran (THF) solvent molecules present in the crystal lattice. The void in **I4TEPM.DMSO** is 956.4 Å<sup>3</sup>, and it consists of a total of 249.2 electrons. Based on the

electron count present in the void, it is hypothesized that there are possibly six dimethylsulfoxide (DMSO) solvent molecules present in the crystal lattice.

Data for the sample **TMS<sub>4</sub>TEPA** was collected at -173°C using microfocused CuK<sub>α1</sub> radiation on a Rigaku Oxford Diffraction (ROD) FR-X rotating anode generator equipped with a HyPix-6000HE hybrid photon counting (HPC) detector and AFC-11 ¼-chi goniometer. Data for the sample **TMS<sub>4</sub>TEPM** was collected at -173°C using microfocused CuK<sub>α1</sub> radiation on a Rigaku Oxford Diffraction (ROD) Synergy-S X-ray diffractometer equipped with a HyPix-6000HE hybrid photon counting detector. Data on the sample **I<sub>4</sub>TEPM.Dioxane** was collected at -173°C using microfocused CuK<sub>α1</sub> radiation on a Rigaku Oxford Diffraction (ROD) Synergy-S X-ray diffractometer equipped with a Pilatus P200K hybrid photon counting (HPC) detector.

For the above three datasets, a data collection strategy to ensure maximum completeness and redundancy was determined using CrysAlisPro.<sup>8</sup> Data processing was done using CrysAlisPro and a multi-scan absorption correction applied using the SCALE3 ABSPACK scaling algorithm.<sup>9</sup> The structure was solved via intrinsic phasing methods using ShelXT<sup>10</sup> and refined using ShelXL<sup>11</sup> in the Olex2 graphical user interface.<sup>7</sup> The space group was unambiguously verified by PLATON.<sup>12</sup> The final structural refinement included anisotropic temperature factors on all non-hydrogen atoms. All hydrogen atoms were attached via the riding model at calculated positions using suitable HFIX commands.

In the structure **TMS<sub>4</sub>TEPA**, a solvent mask was applied in Olex2 to a highly-disordered interstitial CHCl<sub>3</sub> solvent molecule whose behavior could not be satisfactorily modeled. Two of the four pendant –Si(Me)<sub>3</sub> groups were disordered over two positions at ratios of 80:20 with respect to one another. In the structure **TMS<sub>4</sub>TEPM**, a solvent mask was applied in Olex2 to a region of highly-disordered residual electron density presumed to be an interstitial methanol molecule. One of the two pendant –Si(Me)<sub>3</sub> groups from the structure's asymmetric unit, which consisted of half the molecule, was disordered over two positions at a ratio of 89:11 with respect to one another. In the structure **I<sub>4</sub>TEPM.Dioxane**, a solvent mask was applied in Olex2 to a region of highly-disordered residual electron density presumed to be two interstitial water molecules.

**Table S 1: Crystallographic data.**

Code	TMS <sub>4</sub> TEPA	TMS <sub>4</sub> TEPM	I <sub>4</sub> TEPM	I <sub>4</sub> TEPM.THF	I <sub>4</sub> TEPM.DMSO	I <sub>4</sub> TEPM.Dioxane
Formula moiety	C <sub>54</sub> H <sub>64</sub> Si <sub>4</sub>	C <sub>45</sub> H <sub>52</sub> Si <sub>4</sub>	C <sub>33</sub> H <sub>16</sub> I <sub>4</sub>	C <sub>33</sub> H <sub>16</sub> I <sub>4</sub> , (C <sub>4</sub> H <sub>8</sub> O) <sub>2</sub>	C <sub>33</sub> H <sub>16</sub> I <sub>4</sub> , (C <sub>2</sub> D <sub>6</sub> OS) <sub>2</sub>	C <sub>33</sub> H <sub>16</sub> I <sub>4</sub> , (C <sub>4</sub> H <sub>8</sub> O <sub>2</sub> ) <sub>2</sub>
Empirical formula	C <sub>54</sub> H <sub>64</sub> Si <sub>4</sub>	C <sub>45</sub> H <sub>52</sub> Si <sub>4</sub>	C <sub>33</sub> H <sub>16</sub> I <sub>4</sub>	C <sub>41</sub> H <sub>32</sub> I <sub>4</sub> O <sub>2</sub>	C <sub>37</sub> H <sub>16</sub> D <sub>12</sub> I <sub>4</sub> O <sub>2</sub> S <sub>2</sub>	C <sub>41</sub> H <sub>32</sub> I <sub>4</sub> O <sub>4</sub>
Molecular weight	825.41	705.23	920.06	1064.26	1088.39	1096.26
Color, Habit	yellow, plate	colorless, block	yellow, needle	colorless, plate	yellow, needle	colorless, block
Crystal system	triclinic	orthorhombic	monoclinic	tetragonal	monoclinic	monoclinic
Space group, <i>Z</i>	$P\bar{1}$ , 2	<i>Aba</i> 2, 4	<i>I</i> 2/ <i>a</i> , 4	<i>P</i> 4 <sub>2</sub> / <i>mbc</i> , 4	<i>C</i> 2/ <i>c</i> , 4	<i>I</i> 2/ <i>a</i> , 4
<i>a</i> , Å	9.92440(10)	12.4044(2)	19.222(3)	12.1640(13)	26.997(8)	25.3759(4)
<i>b</i> , Å	15.6004(3)	12.5582(2)	7.6455(9)	12.1640(13)	7.325(2)	7.61980(10)
<i>c</i> , Å	18.0918(3)	31.1500(5)	26.324(4)	29.545(3)	25.776(8)	26.6692(5)
$\alpha$ , °	95.5260(10)	90	90	90	90	90
$\beta$ , °	100.2040(10)	90	106.122(7)	90	118.884(16)	117.094(2)
$\gamma$ , °	98.9920(10)	90	90	90	90	90
Volume, Å <sup>3</sup>	2700.63(7)	4852.45(13)	3716.5(9)	4371.6(10)	4463(2)	4590.84(15)
Density, g/cm <sup>3</sup>	1.015	0.965	1.644	1.617	1.620	1.586
Temperature, K	100(2)	100(2)	296(2)	130(2)	130(2)	100.00(10)
Crystal size, mm (min × mid × max)	0.052 x 0.064 x 0.120	0.131 x 0.189 x 0.265	0.035 × 0.045 × 0.450	0.080 × 0.275 × 0.410	0.083 × 0.224 × 0.298	0.106 × 0.149 × 0.169
X-ray wavelength, Å	1.54184	1.54184	1.54178	0.71073	0.71073	1.54184
$\mu$ , mm <sup>-1</sup>	1.242	1.316	26.453	2.880	2.912	21.584
Trans min/max	0.84/1.00	0.75/1.00	0.29/0.75	0.538/0.745	0.577/0.745	0.105/0.330
$\theta_{min}$ , °	4.600	5.681	3.495	1.378	1.723	6.100
$\theta_{max}$ , °	66.590	66.600	69.954	26.279	25.862	67.704
Reflections						
collected	35822	16304	17307	16913	46208	11363
independent	9425	3904	3406	2263	4247	4129
observed	8721	3702	2568	1361	3372	4010
R <sub>int</sub>	0.0267	0.0364	0.0809	0.0740	0.0589	0.0201
Threshold expression	> 2 $\sigma$ ( <i>I</i> )	> 2 $\sigma$ ( <i>I</i> )	> 2 $\sigma$ ( <i>I</i> )	> 2 $\sigma$ ( <i>I</i> )	> 2 $\sigma$ ( <i>I</i> )	> 2 $\sigma$ ( <i>I</i> )

No. parameters	607	253	168	114	206	222
No. restraints	50	7	0	0	0	0
R <sub>1</sub> (observed)	0.0468	0.0439	0.1097	0.0547	0.0325	0.0278
wR <sub>2</sub> (all)	0.1284	0.1263	0.3067	0.1871	0.0803	0.0733
Goodness of fit (all)	1.062	1.044	1.175	1.031	1.084	1.050
$\rho_{\max}, \rho_{\min}, e \text{ \AA}^{-3}$	0.467, -0.594	0.355, -0.191	3.775, -2.262	1.242, -0.760	0.733, -0.951	0.860, -0.920
Completeness to 2 $\theta$ limit	0.986	0.998	0.986	0.998	0.985	0.997

## References

- 1 APEX2 v2013.10-0, © 2013, Bruker Analytical X-ray Systems, Madison, WI.
- 2 COSMO v1.61, © 1999 - 2009, Bruker Analytical X-ray Systems, Madison, WI.
- 3 SAINT v8.34a, © 1997 - 2013, Bruker Analytical X-ray Systems, Madison, WI.
- 4 SADABS v2012/1, © 2012, Bruker Analytical X-ray Systems, Madison, WI.
- 5 SHELXTL v2008/4, © 2008, Bruker Analytical X-ray Systems, Madison, WI.
- 6 Olex2 1.2 - Compiled 2018.04.26 svn.r3504 for OlexSys, GUI svn.r5492.
- 7 Dolomanov, O. V., Bourhis, L. J., Gildea, R. J., Howard, J. A. K. and Puschmann, H., *J. Appl. Cryst.*, **2009**, *42*, 339-341.
- 8 CrysAlisPro, Rigaku Oxford Diffraction, version 171.40.55a, 2019.
- 9 SCALE3 ABSPACK – A Rigaku Oxford Diffraction program for Absorption Corrections, Rigaku Oxford Diffraction, 2017.
- 10 Sheldrick, G. M., *Acta Cryst.*, **2015**, *A71*, 3-8.
- 11 Sheldrick, G. M., *Acta Cryst.*, **2015**, *C71*, 3-8.
- 12 Spek, A. L., *Acta Cryst.*, **2009**, *D65*, 148-155.